Supporting Information

Lapish *et al.* 10.1073/pnas.0804045105

SI Text

Data Acquisition. Custom multielectrode arrays were built using 25-μm-diameter tungsten wires (California Fine Wires) in a 36-gauge silica tube yielding a spacing of 150 μm, arranged in a 2 by 12 matrix with the length spanning the anterior-posterior axis of the ACC (Fig. S1*A*). They were then attached via gold pins to an EIB-27 board and a HS-27 headstage (Neuralynx). A commutator connected the HS-27 to 4 Lynx-8 programmable amplifiers and an EPP-27 patch panel running Cheetah acquisition software (Neuralynx). Signals were sampled at 30,303 Hz filtered between 600–6,000 Hz. Online spike detection signals were amplified 5–10,000 times and thresholds set at 75–125 μV or >3 times the noise amplitude. Clustering was performed through KlustaKwik and Neuralynx's SpikeSort 3D software. They were then manually assigned into clusters by Neuralynx SpikeSort 3D, where multiple parameters were used to effectively visualize clusters with the most often used combination of spike height, trough, and energy. Each cluster was then run through an ISI filter to remove any ISIs <10 ms and any duplicate timestamps from the data set. Data analysis of the clusters was performed by custom written routines in Matlab (MathWorks).

Data Analysis. The following provides additional details and discussion regarding our analysis methods as well as on additional checks we have performed.

MUA space separation. For the smoothing of spike trains, Gaussian functions with 50 ms standard deviation and an integral of one were used.

Solely for the purpose of visualization (Fig. 1), metric multidimensional scaling (MDS) was used to obtain 3D projections of the N-dimensional spaces (N = number of simultaneously recorded cells). Metric MDS finds a lower-dimensional projection of the data points while attempting to preserve the original distances among all points within this projection.

Prototypes of task epochs were computed by averaging across all vectors of that task epoch. In Fig. 1*D*, the difference of each task epoch prototype from the grand average across all task epochs is presented to highlight the differential activities.

To confirm the visually apparent separation among task epochs statistically, a linear classifier was constructed for each trial and pair of task epochs by determining an optimally separating (N-1)-dimensional hyperplane via linear discriminant analysis (e.g., ref. 1). This linear classifier is optimal in the sense of a maximum-likelihood criterion under the assumption that the data are multivariate normally distributed. We chose it for its computational simplicity, which is important given the thousands of surrogates we had to evaluate, its straightforward statistical interpretation, and the absence of any user-defined parameters that might make the process more subjective (as required in many other machine-learning approaches). In Fig. S3, we furthermore show results from two other related statistics, namely the Mahalanobis distance between the group means (which can be viewed as a multivariate extension of d′ in signal detection theory), and the R^2 statistics (explained variance) obtained by multiple regression where class (task epoch) membership is correlated with **iFR**(t). Although classification based on multiple regression is equivalent to that obtained by linear discriminant analysis for the two-category case (see ref. 2, Ex. 4.2, for details), R^2 provides a finer-grained (real-valued) statistics than the classification error.

Because the separation performance will depend on the dimensionality of the space and the numbers of points to be separated (e.g., N points can always be perfectly linearly separated in an (N-1)-dimensional space), surrogates were constructed and used as baseline. A simple way to obtain such surrogates would be to randomly reassign for each comparison the original population vectors to the two task epochs that are to be compared, and then recalculate the classification error. However, as described in *Methods*, we used a more strict criterion to account for potential temporal contingencies within the clouds of points: Pairs of task epochs were first combined, and from these unions of points k contingent segments were randomly drawn, where k is the number of contingent segments for the original task epoch. For instance, there are four correct choice epochs consisting of 5 × 200-ms bins each embedded within the test phase, and hence for a comparison TsC-Ts four segments of five consecutive points are drawn at random from the combined Ts and TsC points. To determine significance across all data sets, the average across the 99 surrogates for each set was obtained and compared to the original classification errors across all data sets by paired t tests with alpha-levels corrected according to the Holm–Bonferroni method (3) [another modified Bonferroni method suggested by Cross and Chaffin (4) yielded identical results].

As noted in the main text, a significant separation among task epochs could on average (across all task epoch pairs) be achieved in ≈40% of all trials, with contributions from all trials and animals. More specifically, for each trial from each animal there was a minimum of 2 significantly differentiated pairs of task epochs and an average of 10.6 (SD = 4.2). Hence, the results are neither specific to one or a few data sets nor to just a few animals, but are a general phenomenon across trials and animals.

As a further check of the results of the separation error analysis, we constructed "metasurrogates" by randomly shuffling the event times within each task phase and subjecting this new data set with randomly defined task epochs to the full analysis. In this case, with only one exception none of the comparisons between shuffled event epochs from the same task phase reached significance.

Low vs. High Behavioral Error Group Comparisons. With regard to the comparison of the two behavioral error groups, we note that the differences among these groups in overall separation (averaged across all epochs) did not reach significance if only training phase-associated comparisons were included (t test, $P > 0.1$), i.e., when delay- and test-phase comparisons were excluded. This was expected, because almost all errors were committed during the test phase, i.e., the two groups were comparable in their performance during the training phase.

We also emphasize that Fig. 3*A* indicates a general breakdown of separation in the high-error group, not one that is confined to those particular choices that were incorrect. As a further test, we compared separation from the basal test phase during correct and incorrect choices for the high-error group only, and found no significant differences between them ($\mu_{\text{TsC-Ts}} = 0.83$, $\mu_{\text{TsI-Ts}} = 0.87$, $P > 0.6$ paired t test), whereas both values were significantly larger than the respective mean for correct choices in the low error group ($\mu_{\text{TsC-Ts}} = 0.61$, $P < 0.05$ for both). Hence, the lack of MUA space separation is related to whether in general many or few behavioral errors were committed but not to particular choices made (e.g., specific arm locations) or whether they are correct or incorrect.

Correlation Analysis. As noted in *Methods*, for comparison of within-task-epoch to across-task-epoch correlations (Fig. S5), equal-time slices were first drawn from all task epochs. More precisely, given that TrC, TrR, TsC, and TsR all consisted of 4 × 5 consecutive bins, 4 × 5 consecutive bins were also drawn from the Tr, Dl, and Ts epochs at random, and TsI was incorporated only if it had at least 4 × 5 bins, which was also the maximum allowed. This procedure ensured that the surrogates drew from every task epoch with equal likelihood. They were now constructed by drawing for each comparison at random 20 bins from the union of time-equalized task epochs, and correlation coefficients were recalculated between time series $iFR_{n,s}(t)$ and $iFR_{m,s}(t)$ for all pairs of neurons n,m, and for each surrogate set s. Original correlations were also recomputed for the time-equalized task epochs, and both original and across-epoch surrogate correlations were corrected by the mean from 99 shuffles (within original or surrogate epochs p or s, respectively), to rule out any potential dependence on absolute firing rates. This process was then repeated 99 times for each dataset, yielding statistically reliable estimates. Note that this is a very conservative test as it retains all correlations among units that may exist across time-equalized task epochs.

All analysis routines were custom-written in Matlab or C++.

Further Analysis Results. To yield some information about the temporal precision of the task epoch-dependent organization into iFR and correlational patterns, the iFR(t) vectors of each neuron were shifted by a random number of bins drawn from a Gaussian distribution with zero mean and standard deviations of σ_{shift} = 1, 3, 6, 8, or 10 bins (100 of such shift surrogates were created for each data set and value of σ_{shift}). Both MUA space separation (averaged across all pairs of epochs) and the average iFR correlations monotonically decayed as the standard deviation σ_{shift} was increased (Fig. S6). For the MUA space separation (Fig. S6*A*), this progressive deterioration became significant (paired t test, $P < 0.05$) from at least σ_{shift} = 3 bins onwards, and continued to significantly deteriorate as σ_{shift} was further increased. This suggests that pattern formation in accordance with task epochs may be a more coarsely grained process, which is not so surprising given that task epochs themselves stretch out across significant periods of time (> = 1 s). Note in particular that even the largest shift (σ_{shift} = 10) should have only little effect on all comparisons across the major task phases (Tr, Dl, Ts), i.e., 19/28 of all epoch-pair comparisons which involve samples from different task phases may still yield significant separation, as the major task phases extend over tens of seconds (explaining the rather small, although significant, effect sizes between consecutive steps in Fig. S6 A). In contrast, iFR correlations started to significantly decay for $\sigma_{shift} \geq 1$ bins (Fig. S6*B*), suggesting that the correlational patterns among units are highly sensitive to a shift of the timing of the instantaneous firing rates. This is even more remarkable as these correlations were averaged across all conditions and neural pairs, including probably many uncorrelated pairs which dilute the overall effect, and as the shifting function had a mean of zero, i.e., both positive and negative (integer number) shifts could occur with equal likelihood, thus potentially preserving many of the original temporal relations in the shift surrogates (at least for small σ_{shift}).

1. Krzanowski WJ (2000) *Principles of Multivariate Analysis* (Oxford Univ Press, Oxford, UK), 2nd Ed.
2. Hastie T, Tibshirani R, Friedman J (2001) *The Elements of Statistical Learning: Data Mining, Inference, and Prediction* (Springer, New York).
3. Holm S (1979) A simple sequentially rejective multiple test procedure. *Scan J Stat* 6:65–70.
4. Cross EM, Chaffin WW (1982) Use of the binomial theorem in interpreting results of multiple tests of significance. *Educ Psychol Measure* 42:25–34.

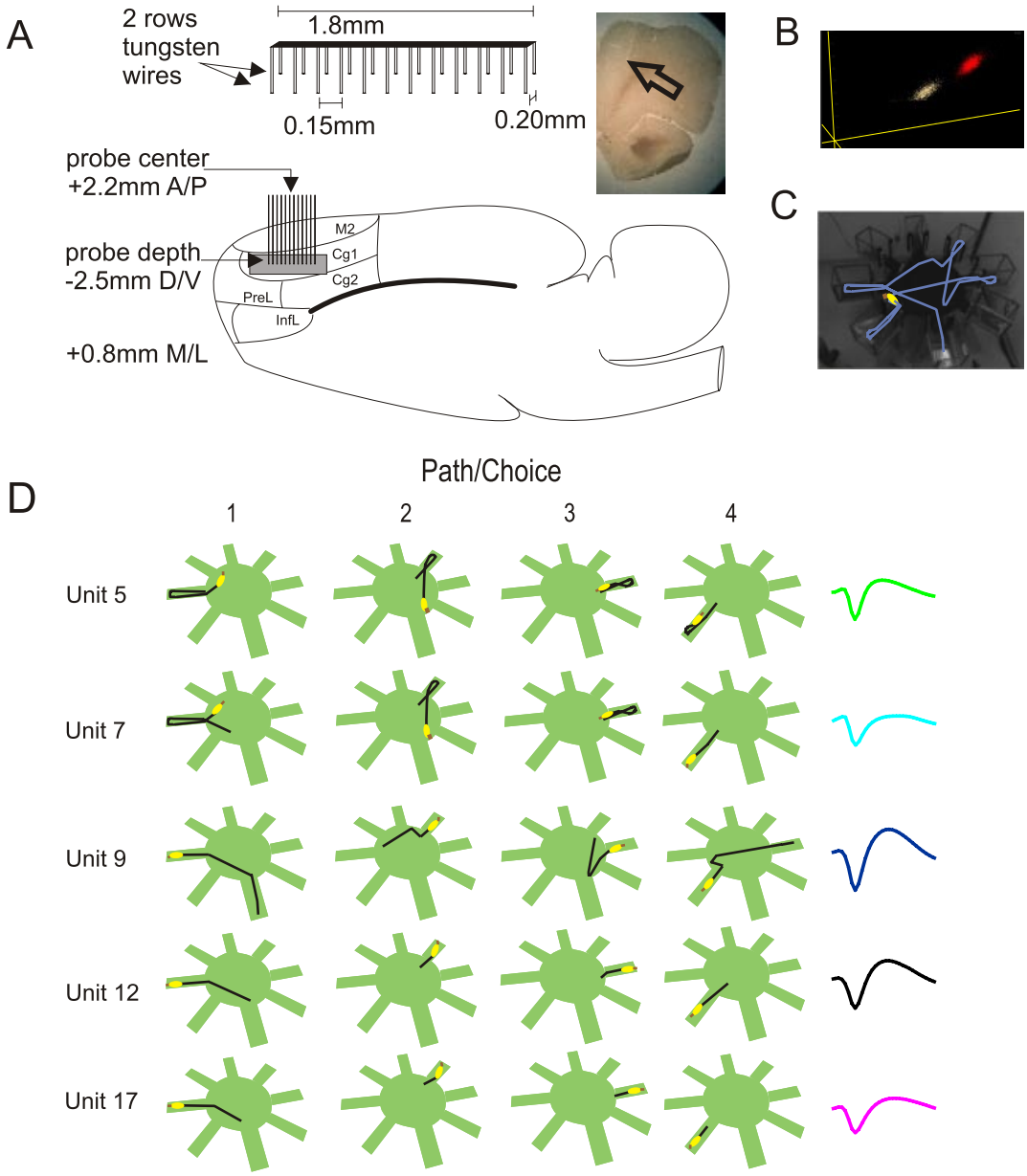

Fig. S1. (*A*) A schematic of the spatial layout of microarrays and a sagittal section of the rat ACC showing the location of recording wires (gray box). A coronal section of rat PFC showing a representative placement with the tip of the arrow identifying the recording site in the ACC (*Upper Right*). (*B*) Three-dimensional projection derived from the waveform properties of two cells isolated from a single wire. (*C*) The path of a rat during the test phase of a representative trial (blue line), and the orientation of the animals' body (yellow oval) and head position (brown square). (*D*) The radial arm maze is shown in green with the path of the animal superimposed in black. In this trial the animal made four correct choices in the test phase and the choices are arranged left to right in a row. The path/position of the animal is shown only for the period when the iFR of one of the five cells deviated significantly from the overall mean iFR. These paths correspond to the test phase iFR shown in Fig. 1*E*.

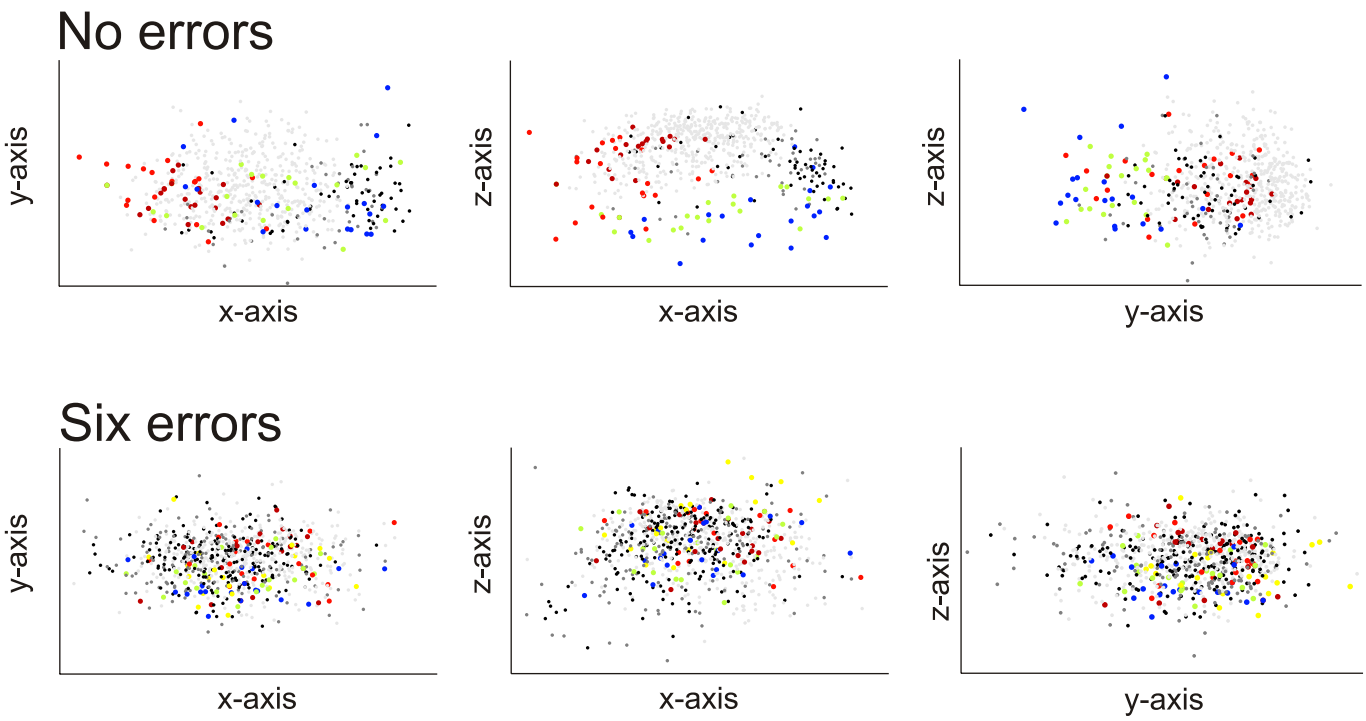

Fig. S2. Two-dimensional plots of each pair of axes from the MUA space plots in Fig. 1 *B* and *C*.

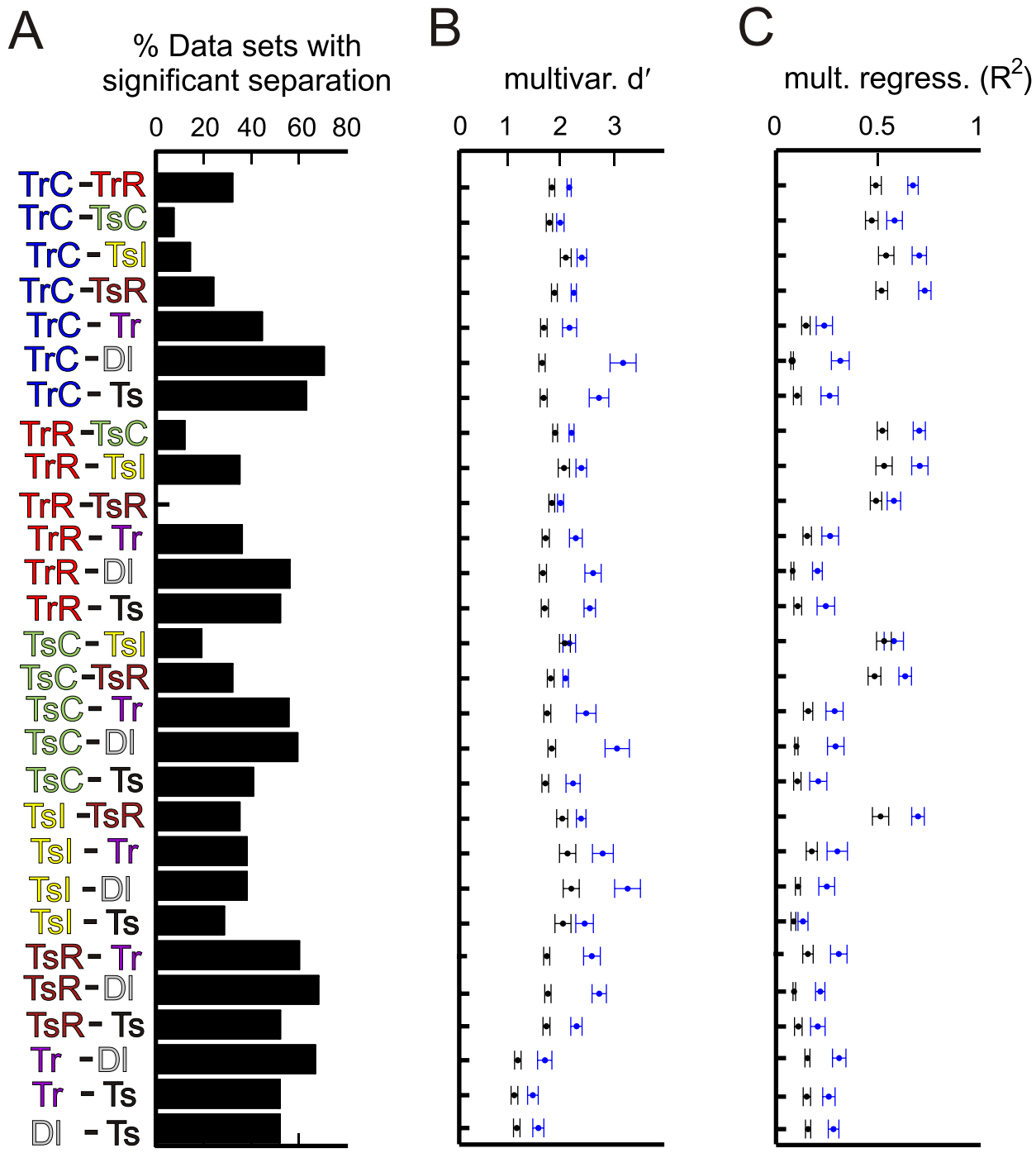

Fig. S3. (*A*) Percentage of individual trials on which a significant separation between task epochs could be achieved, as a function of task epoch-pair comparison. (*B*) Mahalanobis distance between the mean iFR vectors from each pair of task epochs for original and surrogate data (this measure is basically a multivariate equivalent of d′ in signal detection theory). These Mahalanobis distances are significantly larger for the original than for the surrogate data, indicating significantly better separation, for all epoch-pair comparisons except for TsC vs. TsI. This is in perfect agreement with the results of the separation error analysis. (*C*) Likewise, multiple regression R^2 is significantly larger for all original compared to surrogate task-epoch pairs except for the TsC-TsI comparison.

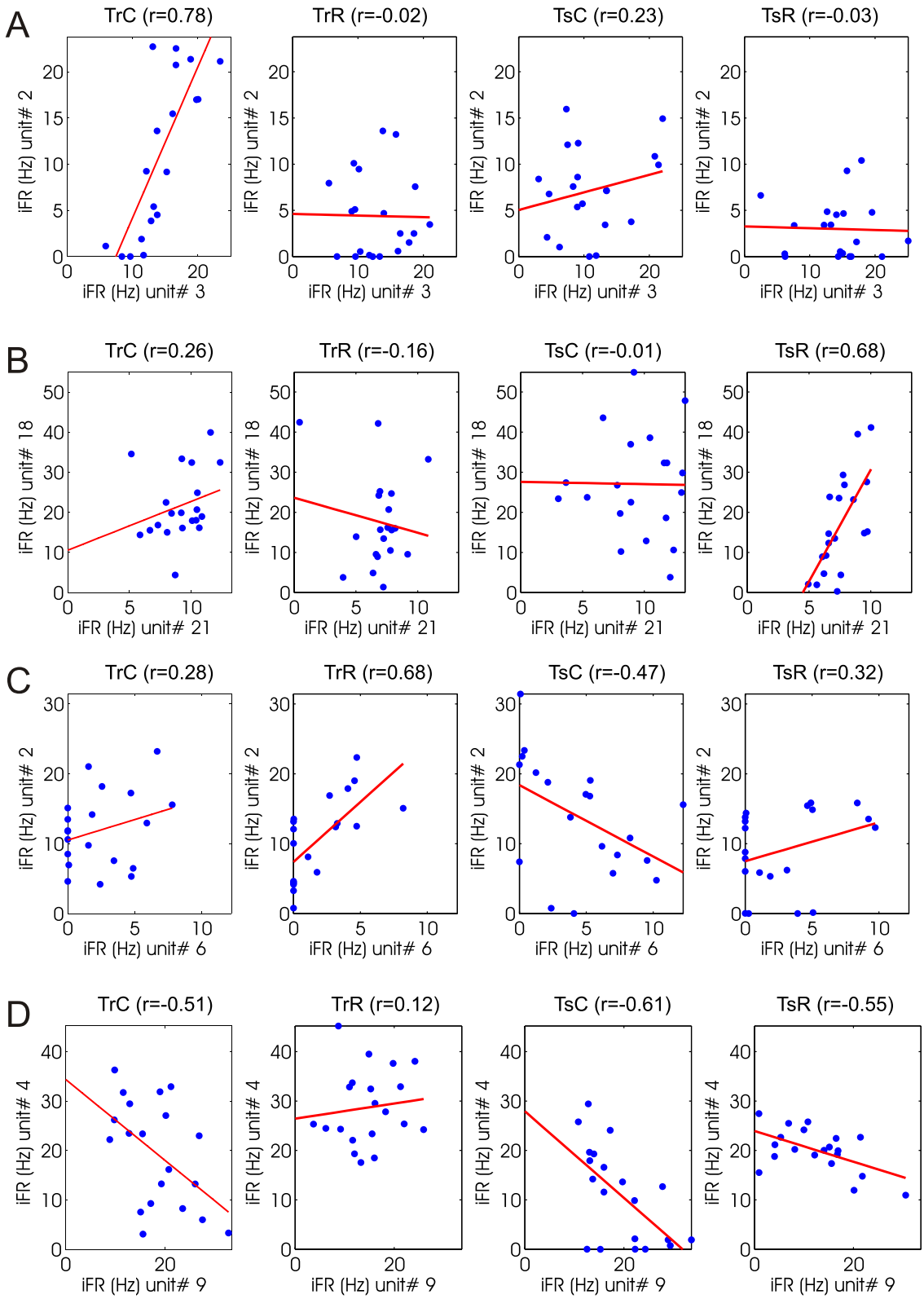

Fig. S4. Four examples of task-epoch-selective iFR correlations. (*A*) Example of a cell pair with a positive iFR correlation during TrC only. (*B*) Example of a cell pair with a positive iFR correlation during TsR only. (*C*) Example of a cell pair with a negative iFR correlation during TsC only, yet a positive correlation during TrR. (*D*) Example of a cell pair with a negative iFR correlation during both correct choice epochs (TrC and TsC, as well as TsR).

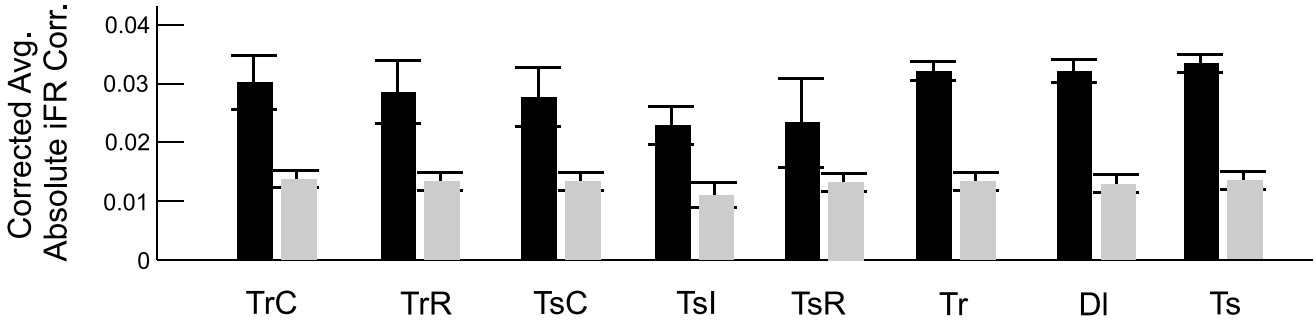

Fig. S5. Comparison of within- to across-task epoch iFR correlations, corrected by mean absolute iFR correlations within shuffled surrogates. Black bars: Average absolute corrected iFR correlation within each of the 8 task epochs. Gray bars: Average absolute corrected iFR correlation within surrogates compiled by recombining segments from all 8 task epochs at random (see Methods for details). Error bars = SEM. Within task epoch correlations were significantly higher than across task epoch correlations for all epochs ($P < 0.005$) except for TsR ($P < 0.1$).

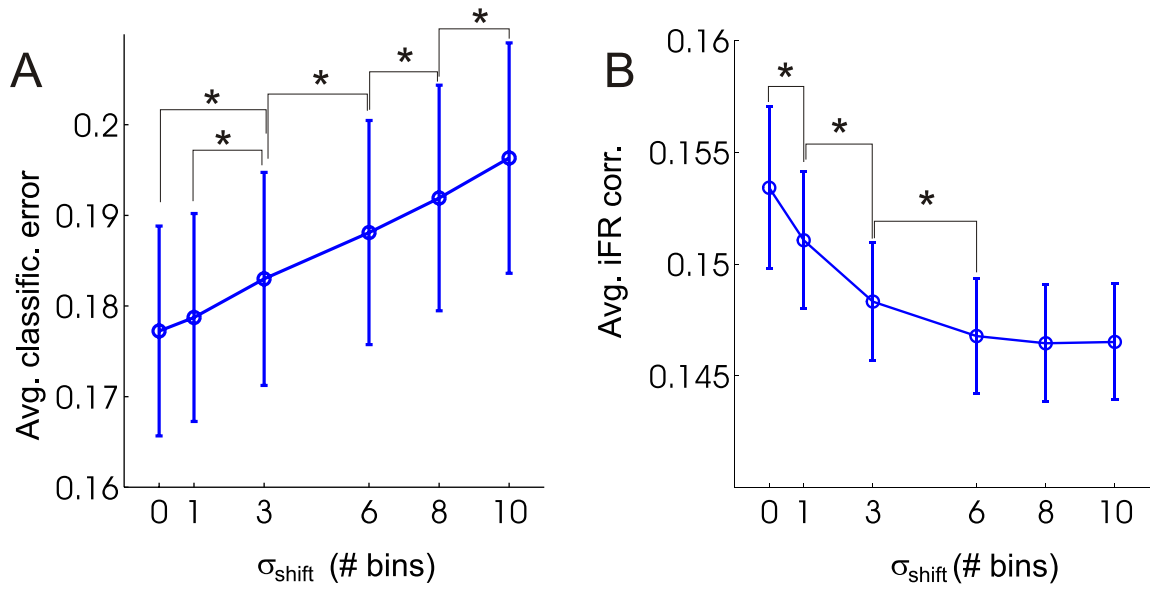

Fig. S6. (*A*) Deterioration of MUA space separability as a function of the degree of temporal shifting of the neural iFR(t) vectors (in terms of the standard deviation, σ_{shift}, of the average shift in units of 200 ms iFR bins). The differences to the baseline condition ('0', the original data) became significant for $\sigma_{shift} \geq 3$, and each difference among consecutive steps became significant as well. (*B*) Decay of absolute iFR correlations as a function of σ_{shift}. Correlations were averaged across *all* pairs of each data set (likely to include many uncorrelated pairs) and all task epochs. All differences to the original data were significant for $\sigma_{shift} \geq 1$, and the first couple of consecutive differences were significant as well as indicated by the stars. Error bars = SEM.

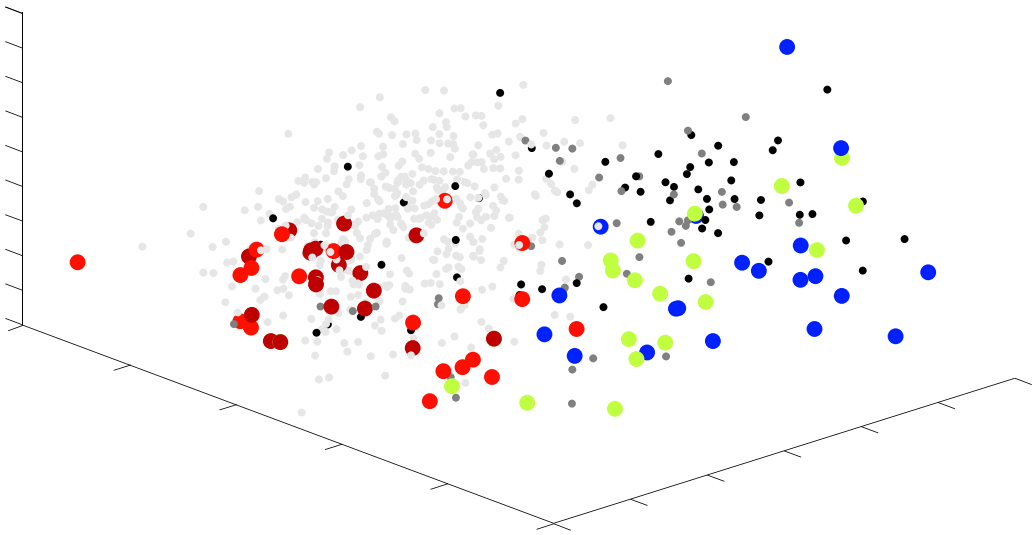

Movie S1. 3D rotational animation of Fig. 1*B*.

Movie S1(AVI)

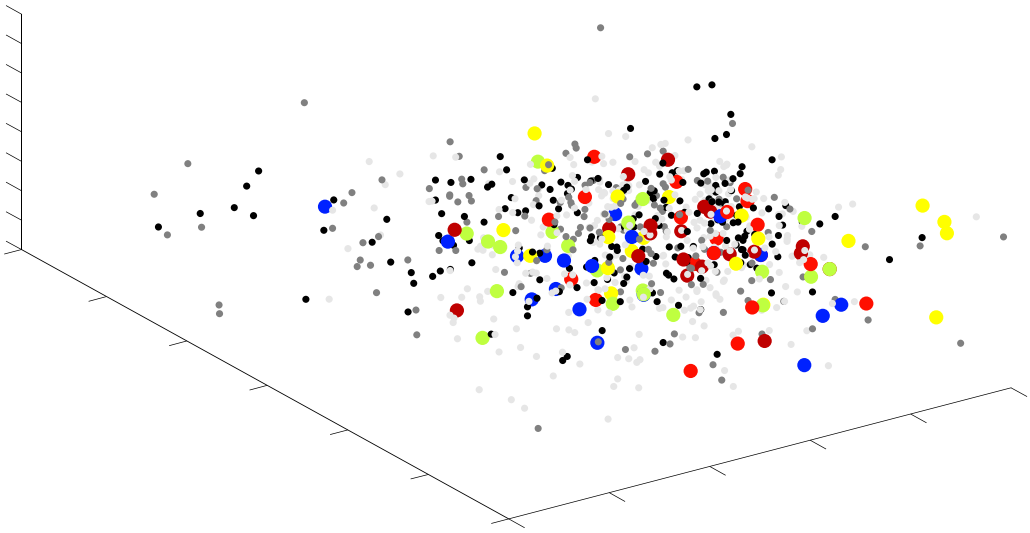

Movie S2. 3D rotational animation of Fig. 1C.

Movie S2(AVI)